

Advances in InGaN-based RGB micro-light-emitting diodes for AR applications: Status and perspective

Cite as: APL Mater. 12, 080901 (2024); doi: 10.1063/5.0222618

Submitted: 9 June 2024 • Accepted: 29 July 2024 •

Published Online: 14 August 2024



View Online



Export Citation



CrossMark

Panpan Li,¹ Jacob Ewing,¹ Matthew S. Wong,¹ Yifan Yao,¹ Hongjian Li,^{1,a)} Srinivas Gandrothula,¹ Jordan M. Smith,¹ Mike Iza,¹ Shuji Nakamura,^{1,2} and Steven P. DenBaars^{1,2}

AFFILIATIONS

¹ Materials Department, University of California, Santa Barbara, California 93106, USA

² Department of Electrical and Computer Engineering, University of California, Santa Barbara, California 93106, USA

^{a)} Author to whom correspondence should be addressed: hongjianli@ucsb.edu

ABSTRACT

Micro-light-emitting diodes (μ LEDs) are gathering significant interest as a technology for emerging micro-displays. However, μ LEDs encounter numerous obstacles, including size-dependent efficiency loss, poor efficiency of red μ LEDs, and challenges associated with the mass transfer and integration of full-color μ LEDs. These issues become more acute in ultra-small μ LEDs ($<5\text{ }\mu\text{m}$), which were required by the augmented reality (AR) displays. Here, we discuss the principal challenges faced by μ LEDs and explore the possible solutions. We highlight recent advances in InGaN-based RGB μ LEDs tailored for AR displays. In particular, we discuss the advancements in ultra-small InGaN μ LEDs scaled down to $1\text{ }\mu\text{m}$, the developments in InGaN red μ LEDs, and the implementation of tunnel junction-based cascaded InGaN μ LEDs for monolithic integration.

© 2024 Author(s). All article content, except where otherwise noted, is licensed under a Creative Commons Attribution (CC BY) license (<https://creativecommons.org/licenses/by/4.0/>). <https://doi.org/10.1063/5.0222618>

I. THE CRITICAL CHALLENGES OF μ LEDS FOR AR APPLICATION

Since micro-light-emitting diodes (μ LEDs) were first demonstrated by Jiang's group in Texas University,¹ the rise of next-generation human-computer interaction platforms, such as augmented reality (AR), virtual reality (VR), and mixed reality (MR), has spurred significant interest in μ LEDs display technology. These applications demand requirements such as ultra-high resolution for head-up displays (HUD) and low power consumption for battery-operated mobile devices.^{1–3} μ LED displays stand out due to their exceptional luminance, long lifetime, high efficiency, and wide color gamut. Nevertheless, several critical challenges must be addressed to fully leverage their capabilities in AR displays.

A. Ultra-small-size μ LEDs required for AR displays

Reducing the μ LEDs or pixel size is crucial for AR display with enhanced resolution and compactness. HUDs for AR applications

demand significantly higher pixel densities since they are positioned much closer to the user's eyes and have a smaller form factor than traditional display systems. Figure 1 shows the smallest necessary μ LED pitch distances to achieve specific resolution across various field of views (FOVs), which in in commercial headsets typically range from 60° to 100° .⁴ Assuming the distance between the μ LEDs display and human eyes L_D is 20 mm, to achieve the retinal resolution (~60 pixel per degree) routinely achieved on most smartphones and tablets nowadays, the pixel pitch needs to be smaller than $6\text{ }\mu\text{m}$, which is the maximum permissible distance between the centers of adjacent pixels.⁴ In addition, the mesa of subpixel μ LEDs mesa size must be reduced further to accommodate inter-pixel electrodes and/or optical components. Therefore, it is imperative to develop highly efficient ultra-small ($<5\text{ }\mu\text{m}$) μ LEDs for AR displays.⁵ Furthermore, in projection-based architectures, where the light from the source (e.g., μ LED) needs to be coupled to a waveguide, there is increased need for a smaller pixel size since smaller point sources are easier to couple.

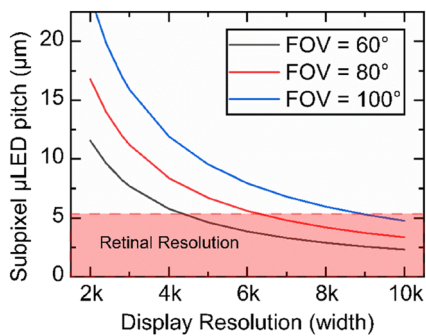


FIG. 1. Subpixel μLED pitch for near-eye display system with field of views (FOVs) of 60° , 80° , and 100° . The subpixel pitch needs to be less than $5\text{ }\mu\text{m}$ to achieve retinal resolution regardless of FOVs.⁴

B. Size-dependent efficiency loss in μLEDs

Highly efficient μLEDs are desirable because they can deliver high luminance and low heat generation, essential to compact, battery-operated HUD devices. However, the efficiency of III-nitride and AlInGaP-based μLEDs decreases by scaling down the device sizes.^{6–12} This size-dependent efficiency loss was commonly attributed to sidewall defects of the active region caused by the dry etch process, which act as Shockley–Read–Hall (SRH) non-radiative recombination sites and path for leakage.^{10–12} Issues worsen with the size reduction, particularly in ultra-small μLEDs ($<5\text{ }\mu\text{m}$) needed for AR displays, as the surface-area-to-volume ratio increases (Fig. 2).^{10,13,14}

SRH nonradiative recombination centers, such as sidewall defects, are introduced during the dry etching process that defines the light-emitting area (mesa).^{15–18} The AlInGaP material system has a greater minority diffusion length, and thus more severe device degradation is observed in AlInGaP μLEDs. In addition, the diffusion length of carriers in AlInGaP is longer compared to InGaN, making it easier for carriers to reach the SRH centers on the mesa

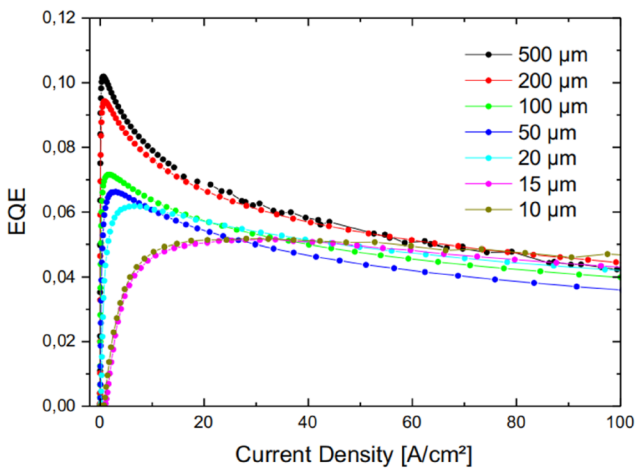


FIG. 2. Degradation of EQE in InGaN μLEDs with respect to device sizes. Reproduced from J. Lumin. **191**, 112 (2017) with permission from Elsevier.

sidewalls. InGaN has a relatively low carrier diffusion length, which means that even if SRH centers exist on the sidewall, they will not see as much current. Furthermore, the diffusion length decreases with higher fraction of indium in the active region, suggesting that the influences of sidewall damage and surface recombination lessen for long-wavelength devices in a III-nitride material system. The extrinsic SRH nonradiative recombination from sidewall damage and surface recombination is the main limitation to the performance of μLEDs, where the effective SRH nonradiative recombination coefficient increases for device dimensions smaller than $40\text{ }\mu\text{m}$.^{15,19} This damage manifests in both the optical and electrical characteristics of μLEDs, including a noticeable reduction in peak EQE, decreased optical power, increased leakage current, and a degraded ideality factor.^{13,20–24} Therefore, mitigating or eliminating the effects of sidewall damage is critical to enhance the performance of μLEDs.^{20,23} It is feasible to mitigate some of the sidewall defects through milder etching techniques²⁵ and subsequent post-etching treatments.^{26,27} These details will be explored in greater detail in Sec. II.

C. Low efficiency of red μLEDs and the full-color scheme

The full-color display operates on the principle of three primary colors—red (R), green(G), and blue(B)—which can be combined to produce all colors in nature. In μLED displays, each pixel contains a set of RGB subpixels with controllable brightness levels. Currently, the poor efficiency of ultra-small red μLEDs is one major concern in full-color display.

AlInGaP^{28–30} or quantum dot (QD) color conversion layers^{31–33} are commonly used for red emission, but they both present notable challenges. AlInGaP materials exhibit surface recombination velocities that are one or two orders of magnitude higher than those of InGaN, causing severe size-dependent EQE loss in smaller μLEDs.^{21–34} The EQE of AlInGaP red μLEDs reduces dramatically by decreasing the device size. Ultra-small size AlInGaP red μLEDs show a much lower efficiency, which cannot satisfy the requirement for AR displays. In addition, the high temperature stability is poor in AlInGaP red μLEDs.³⁵ QDs suffer from degradation issues, and undesirable thickness and patterning results in increasing difficulty when the pixel width is smaller than $10\text{ }\mu\text{m}$.^{36,37} It is also difficult to achieve directional emission with QD conversion, which is a problem for project-based displays. In either case, incorporating QDs or AlInGaP for red emission leads to complex and expensive manufacturing steps, hindering the development of full-color μLEDs displays.

Ideally, all RGB subpixels would be made from the same material to facilitate a simpler integration process and supply chains. The only semiconductor system with bandgap energy that can cover the entire visible spectrum is InGaN. While blue LEDs perform well, the developing longer wavelengths InGaN-based LEDs face challenges due to epitaxial difficulties from the larger lattice mismatch between the InGaN active region and low growth temperature.^{38–40} The large polarization fields in InGaN further limit both radiative recombination efficiency and injection efficiency.^{40–42} These challenges become more pronounced for InGaN red emitter.⁴³ Therefore, highly efficient red InGaN μLEDs are crucial for achieving full-color self-emissive μLED displays. These topics will be subsequently explored in Sec. III.

D. Mass transfer and integration of full-color μ LEDs

Despite significant progress in the growth and fabrication of μ LEDs, one of the major obstacles for their use in large commercial production of display systems is mass transfer and chip integration. For a display with a resolution of 4 K (3840×2160), nearly 25×10^6 subpixel μ LEDs must be transferred from the growth wafer and integrated onto the driver chip.⁴⁴ This requires high throughput mass transfer technology, which surpasses the capabilities of traditional “pick and place” techniques. For a full-color micro-display, integrating three different color RGB μ LEDs from three different epitaxy wafers increases the complexity and cost and typically results in lower yield. Many approaches have been proposed and demonstrated to mass transfer individual μ LEDs, including laser lift-off, fluidic assembly, electrostatic arrays, magnetic arrays, elastomer stamp, and roll-to-roll processes.^{44–49} Overall, a successful mass transfer technology for μ LEDs-based AR displays achieve a high transfer yield (>99.99%), a rapid transfer rate (> 10×10^6 per hour), and cause minimal damage to fragile μ LEDs, all of which continue to pose significant challenges. A novel technique using tunnel junctions (TJ)⁵⁰ to enable the integration of μ LEDs will be discussed in Sec. IV.

II. HIGHLY EFFICIENT ULTRA-SMALL InGaN-BASED μ LEDs

Ultra-small-size μ LEDs essential for AR displays, face efficiency degradation and notably low EQE due to nonradiative recombination related to sidewall damages. Here, we examine potential solutions to recover the efficiency loss. In addition, ultra-small highly efficient InGaN μ LEDs scaled down to $1 \mu\text{m}$ were presented.

A. Recovering the efficiency of μ LEDs by sidewall treatments

It is important to develop a method that suppresses or eliminates the impacts of sidewall damage.¹⁶ Since sidewall damage is a consequence of the etching process, various strategies have been explored to mitigate this issue, including the use of specific etching techniques, such as neutral-beam etching, or etch-free current confinement methods, such as ion implantation. Nevertheless, scaling

these many of these methods for reliable mass production remains challenging due to potential reliability concerns.^{24–26}

The use of dielectric sidewall passivation by atomic layer deposition (ALD) has been extensively employed to suppress the impacts of surface recombination and sidewall defects in III-nitrides and AlInGaP μ LEDs.^{17,27,28} ALD sidewall passivation offers several advantages, such as flexibility in choosing dielectric materials, excellent conformal coverage, and superior material quality compared to other dielectric deposition methods,¹⁸ such as plasma-enhanced chemical vapor deposition (PECVD) or RF sputtering, which did no significant improvement in the performance of μ LEDs (Fig. 3).⁵¹ On the other hand, it has been shown that ALD sidewall passivation enhances the optical and electrical characteristics of μ LEDs by reducing the trap states and nonradiative recombination centers.⁵² In addition, researchers have demonstrated that the deposition details, including film thickness and dielectric material, would have significant effects on the device performance.^{53,54} Research has shown both plasma-based and thermal-based ALD techniques to have been used for effective sidewall passivation in μ LEDs, leading to improved device characteristics.

Other than ALD sidewall passivation, chemical treatment is another common method to mitigate the sidewall defects in LEDs. It has been shown that there is a strong correlation between the chemistry related to the deposition mechanism of ALD, the chemical used, and the device performance.^{55,56} The results present that surface chemistry of the device plays an essential role in addressing surface defects.^{57,58}

For III-nitride materials, several chemicals including potassium hydroxide (KOH), tetramethylammonium hydroxide (TMAH), ammonium sulfide, and phosphoric acid have been utilized to alleviate the impacts of sidewall damage. The explanation for the enhancement in device performance is likely due to oxidation or other surface chemistry in the atomic level, which serve to passivate dangling bonds and to remove defective material. Chemical treatments have shown promise in reducing the impacts of etch damage. When combined with ALD sidewall passivation, size-independent EQE characteristic for devices ranging from 100×100 to $10 \times 10 \mu\text{m}^2$ has been achieved.^{13,59,60} Moreover, chemical treatment provides benefit in light extraction efficiency by the formation of *m*-plane faceted sidewalls.^{61,62} This sidewall treatment technique has enabled highly efficient InGaN μ LEDs, where device efficiency is limited by

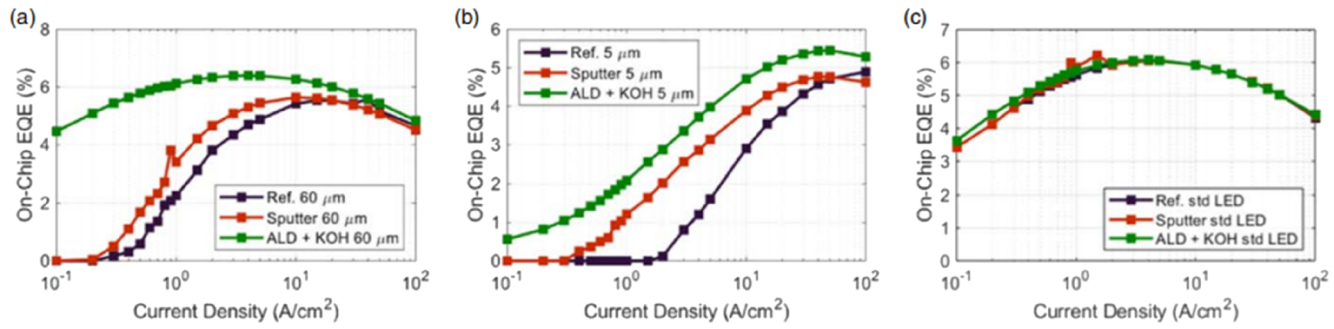


FIG. 3. EQE characteristics of InGaN-based μ LEDs with different sidewall treatments. Reproduced from Wong et al., Jpn. J. Appl. Phys. **63**, 040903 (2024). Copyright IOP Publishing Ltd. All rights reserved.

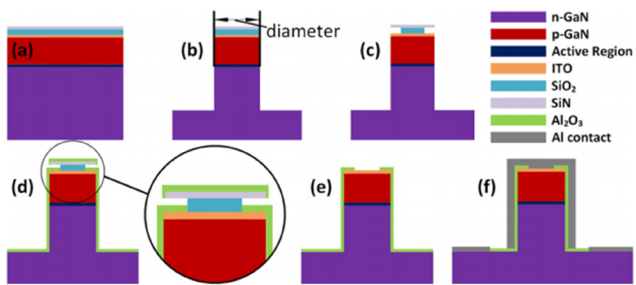


FIG. 4. Schematic self-alignment process of 1 μm InGaN μ LEDs. Reproduced from Smith *et al.*, Appl. Phys. Lett. **116**, 071102 (2020) with the permission of AIP Publishing LLC.

the intrinsic material quality rather than sidewall defects from etch damage.

B. Scaling InGaN μ LEDs down to 1 μm

By reducing pixel size to 1 μm , the resolution and compactness of μ LED displays can be significantly enhanced, which is crucial for AR devices where space and image clarity are paramount. In projection-based display architecture, the light needs to be coupled to waveguides, which will require very small point sources. Since the efficiency of InGaN-based μ LEDs can be fully recovered through proper sidewall passivation and chemical treatments, it is feasible to achieve ultra-small highly efficient InGaN μ LEDs. The first investigations of InGaN μ LEDs with a diameter of only 1 μm was reported by Smith *et al.* from UCSB, who developed a self-aligned fabrication process (Fig. 4).¹⁸ This process involved forming a self-aligned undercut structure on top of the mesa, which was then lifted off after depositing an AlO_x dielectric layer to expose the indium tin oxide (ITO) on top of the mesa. This process offers several advantages, as follows: (i) problem of p-contact misalignment is avoided; (ii) P-contact damage from dry etching can be eliminated; and (iii) light extraction efficiency can be increased by flip-chip configuration with ITO covering the whole mesa.

Ley *et al.* from UCSB demonstrated that the EQE of InGaN blue μ LEDs can be increased from 8.5% to 13.5% by KOH treatment when the diameter was reduced from 20 to 2 μm [Fig. 5(a)] due to enhanced light extraction.⁶² Smith *et al.* found that InGaN green μ LEDs had shown a less size-dependent EQE droop, which was attributed to the decreasing diffusion lengths in the InGaN quantum wells (QWs) with a higher indium composition [Fig. 5(b)].⁹ Reduced surface recombination with increasing indium content in InGaN QWs can also be related to carrier localization near indium-rich regions. Hence, ultra-small InGaN-based native full-color μ LEDs show significant potential from the AR applications. Exploring highly efficient ultra-small InGaN red μ LEDs scaled down to 1 μm is an on-going project at UCSB, and the results will be published soon.

III. ADVANTAGES AND PROGRESS OF InGaN-BASED RED μ LEDs

InGaN μ LEDs are emerging as viable alternative red-light sources due to their simpler technology and compatibility with mass production for displays. This section will explore the advantages of InGaN red μ LEDs and discuss their recent progress.

A. Advantages of InGaN red μ LEDs

There are the following three important size-dependent effects that improve InGaN μ LEDs efficiency: (i) surface recombination velocity is reduced as indium content increases in InGaN μ LEDs; (ii) non-radiative recombination related to sidewall damage in μ LEDs can be suppressed by proper sidewall passivation and chemical treatments; and (iii) light extraction efficiency increases as μ LEDs size decreases. Li *et al.* from UCSB first reported size-independent EQE varied from 2.4% to 2.6% in InGaN red μ LEDs when the device size reduced from 100×100 to $20 \times 20 \mu\text{m}^2$ (Fig. 6).⁶³ A clear comparison of normalized EQE vs μ LEDs size between InGaN and AlInGaP red μ LEDs points out that it is feasible to achieve ultra-small (<5 μm) highly efficient red μ LEDs using InGaN materials instead of the traditional AlInGaP.

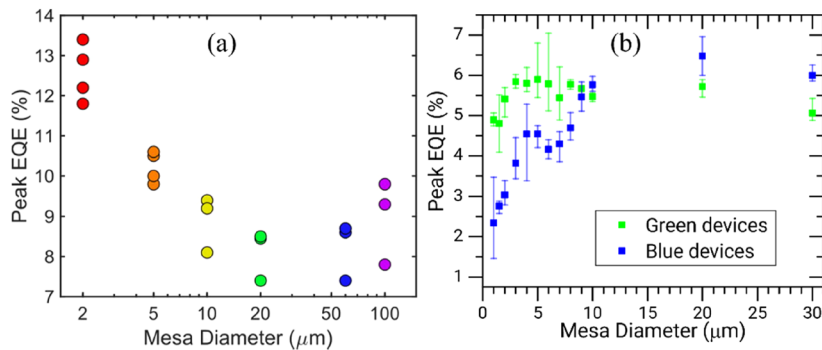


FIG. 5. (a) Peak EQE of 2 to 100 μm blue μ LEDs. Reproduced from Ley *et al.*, Appl. Phys. Lett. **116**, 251104 (2020) with the permission of AIP Publishing LLC. (b) Peak EQE as a function of mesa diameter for InGaN blue and green μ LEDs. Reproduced from Smith *et al.*, Appl. Phys. Lett. **116**, 071102 (2020) with the permission of AIP Publishing LLC.

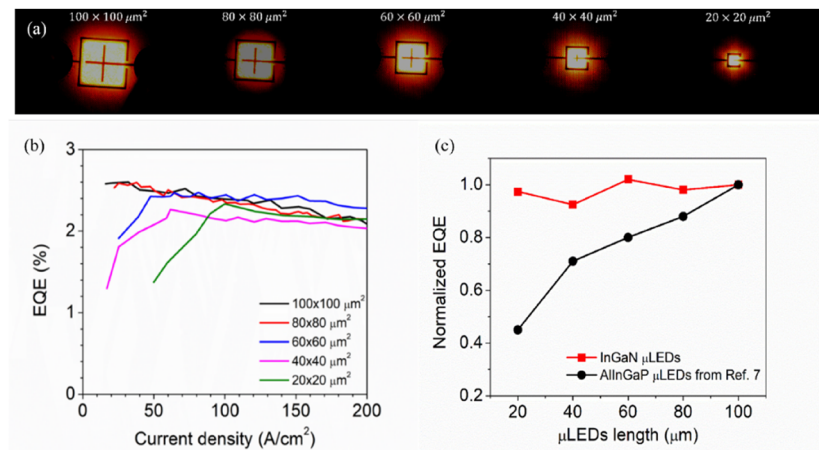


FIG. 6. (a) Microscope images of InGaN red μLEDs; (b) EQE curves of InGaN red μLEDs; and (c) normalized peak EQE for different sizes of InGaN and AlInGaP red μLEDs. Reproduced from Li *et al.*, Appl. Phys. Lett. **119**, 081102 (2021) with the permission of AIP Publishing LLC.

Another advantage of InGaN red μLEDs is their superior temperature robustness compared to AlInGaP red μLEDs. Lee *et al.* reported that the output power and EQE of AlInGaP red μLEDs decreased by more than 70% when the operating temperature increased from room temperature to 400 K due to carrier leakage and reduction of injection efficiency.⁶⁴ In contrast, the UCSB team showed that the EQE of InGaN red μLEDs was reduced by 28% when the operating temperature increased to 400 K.^{65,66} The largely alleviated thermal efficiency droop in the InGaN red μLEDs is caused

by the higher barrier height in the active region. Therefore, InGaN red μLEDs are much more suitable when the μLEDs were operated at various temperature.

B. Recent progress of InGaN red μLEDs

Recent research advances in this area include novel designs for the active region design;^{67–72} V-pit engineering and strain relaxation technologies, such as growing on InGaN compliant

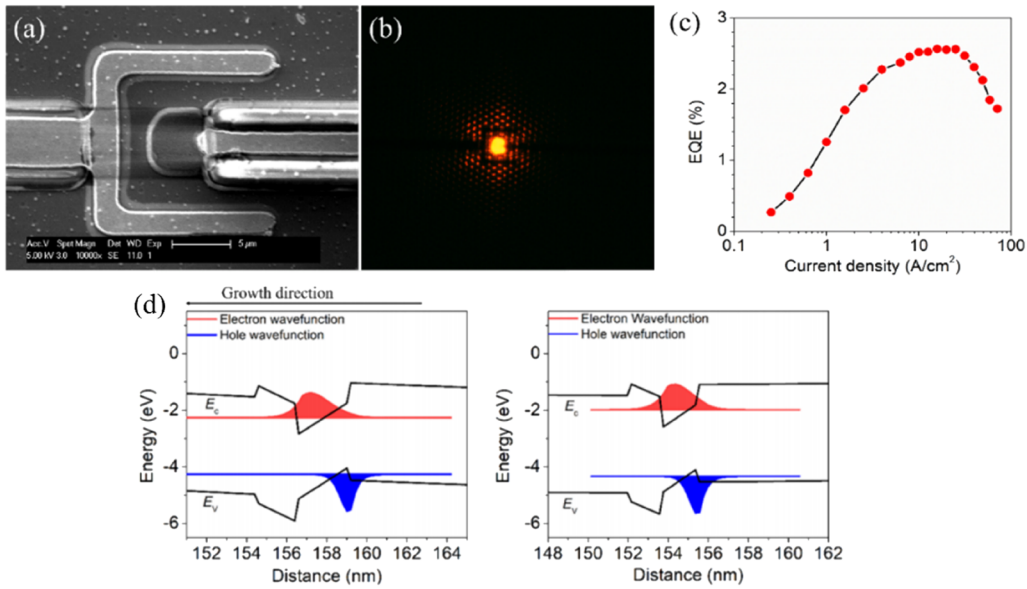


FIG. 7. (a) SEM and (b) microscope image of 5 × 5 μm² μLED; (c) EQE vs current density. Reproduced from Li *et al.*, Appl. Phys. Lett. **120**, 041102 (2022) with the permission of AIP Publishing LLC. (d) Electron–hole wavefunctions overlap in the GaN/InGaN/AlGaN MQWs. Reproduced with permission from ACS Photonics **10**, 1899 (2023). Copyright 2024 American Chemical Society.

pseudo-substrate,^{73–76} nano-porous GaN templates,⁷⁷ and InGaN strain-relaxed template (SRT).^{78,79}

In 2014, Hwang *et al.* from Toshiba reported 629 nm InGaN red LEDs grown on a patterned sapphire substrate (PSS) using a $\text{Al}_{0.9}\text{Ga}_{0.1}\text{N}$ cap layer on top of InGaN red QWs. The work from Toshiba showed that AlGaN caps could help prevent indium desorption from the QWs and utilized multistep GaN QBs and high TMIn flows to improve the red LED performance. These growth approaches are now used by most red InGaN growth efforts.⁸⁰ In 2020, Iida *et al.* from KAUST demonstrated InGaN red LEDs growing on PSS with a very thick n-GaN under layer, achieving a peak EQE of 1.6% for the 633 nm red LEDs.⁷⁰ Recently, the KAUST group increased the EQE of the InGaN red μ LEDs to 4.5%.⁷²

The UCSB team has contributed significantly to the development of InGaN red μ LEDs grown on PSS.^{5–7} In 2021, the EQE InGaN red μ LEDs are size-independent with a value across 2.4%–2.6% for various μ LEDs sizes. This group was the first to realize ultra-small $5 \times 5 \mu\text{m}^2$ efficient 609 nm InGaN amber μ LEDs with a peak EQE of 2.6% [Figs. 7(a)–7(c)], alongside a remarkably small leakage current of 10^{-9} A at -5 V.⁸¹ In contrast, the EQE of ultra-small AlInGaP red μ LEDs is only on the order of 0.1% due to numerous SRH nonradiative recombinations, which is one order lower than the reported InGaN amber μ LEDs.⁸²

Recently, the UCSB group managed to boost the EQE to 6% for InGaN red μ LEDs by utilizing an InGaN/AlGaN/GaN multiple quantum wells (MQWs) structure with 1.9 nm thin QWs.^{67,83} Significant enhancement of internal quantum efficiency (IQE) was achieved due to the increased overlap of electron–hole wavefunctions overlap within the QWs [Fig. 7(d)]. Notably, the EQE values reported from UCSB were measured using an integrating sphere, providing more accuracy than the power meter techniques commonly seen in the literature. Chen *et al.* reported InGaN red LEDs with a peak EQE of 7%.⁴⁰ Lee *et al.* from Samsung achieved InGaN red μ LEDs with a peak EQE of 10.5% using an AlGaN interlayer within MQWs.⁶⁸ The process of growing InGaN red μ LEDs on PSS aligns well with the established processes for blue and green μ LEDs, facilitating easier scaling to mass production. Moreover, Jiang *et al.* from Xiamen University reported a novel technology to epitaxially design InGaN LEDs using the most advanced and cutting-edge machine learning, which opens a new window and accelerates the future development of highly efficient InGaN red μ LEDs.⁸⁴

Jiang *et al.* from Nanchang University showcased the use of V-pits-induced 3D *pn* junctions, which are beneficial for screening dislocations and increasing hole injection efficiency (Fig. 8).⁶⁹ V-pit (or V-defect) engineering is critical for achieving high wall plug efficiency (WPE) in red LEDs, which is ultimately the most important efficiency metric for displays. One of the biggest challenges with long wavelength III-N LEDs are the increased polarization barriers that greatly hinder the vertical transport of carriers making it very difficult for the carriers to reach the QWs.⁸⁵ This especially impacts the forward voltage of the LEDs, which is inversely related to the WPE. V-defects have six {101·1} semipolar sidewalls and are typically formed on threading dislocations, which occur naturally in GaN.⁸⁶ In 2020, the Nanchang group developed 621 nm InGaN red LEDs that reached a peak WPE of 16.8%.⁸⁷ This year Lumileds reportedly broke the Nanchang efficiency record with a WPE of 18% at a dominant wavelength of 623 nm in InGaN red LEDs, representing a significant process in exploring InGaN red emitters.⁸⁸

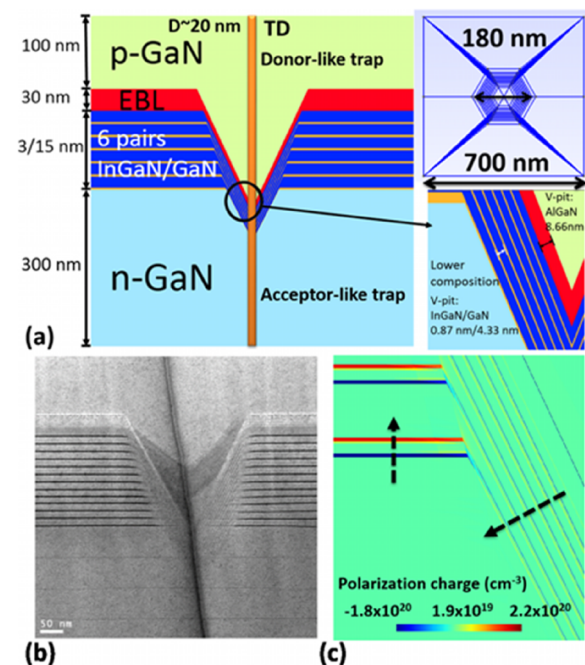


FIG. 8. (a) Cross-sectional view and detailed dimensions of the simulation structure for the V-pit LED. (b) TEM of the MQWs; (c) calculated polarization charge distribution (cm^{-3}).⁸⁹

During growth, the semipolar planes of the V-defects have a significantly lower uptake of In and Ga, leading to thinner sidewalls with significantly less indium.⁹⁰ It is the lower In%, thinner wells, and lower polarization on the semipolar sidewalls that provide beneficial pathways for carrier injection. Recent work from UCSB and KTH Royal Institute of Technology in Sweden has provided compelling experimental evidence of lateral carrier injection in V-defect LEDs.⁹¹ It is critical that the V-pits form below the active region, such that this beneficial sidewall structure can properly form during epitaxy. If the V-pits form during active region growth, they tend to create non-radiative pathways that degrade device efficiency.⁹²

V-pit engineering on PSS has proven to be slightly more difficult due to the lower TDD and higher fraction of pure-edge TDs compared to mixed TDs. Ewing *et al.* from UCSB reported a packaged EQE of 6.5% and 3.5% WPE at an emission wavelength of 600 nm for standard 0.1 mm^2 LEDs grown on PSS, but the V-defect density ($1 \times 10^8 \text{ cm}^{-2}$) in these LEDs was insufficient for complete lateral injection and low voltage operation.⁹³ The simulation results show that the voltage of LEDs with V-pits is highly related to the density.^{89,94} This is due to the relatively short lateral diffusion length of carriers in GaN, which is ~ 100 nm.⁹⁵ The short diffusion lengths mean that the V-defect density needs to be $\sim 10^9 \text{ cm}^{-2}$ to achieve high WPE. On-going work at UCSB is developing novel preparation layers to nucleate V-defects on pure edge dislocations and optimize the V-defect density through novel half-loop formation.⁹⁶

V-pit engineering and lateral injection is a promising technology to achieve highly efficient InGaN red LEDs. However, at

ultra-small size, there are two additional challenges to be considered when using V-pits-based lateral injection: the distribution uniformity and the dimension of the V-pits. Because the distribution is determined by the threading dislocation distribution, it is random and sometimes clustered. This should not be much of an issue for typical μ LEDs down to $\sim 5 \mu\text{m}$. However, for ultra-small μ LEDs, when the mesa size is on a similar length scale of the V-pits, random distribution may become an issue. This is especially true for a μ LED scaled down to $1 \mu\text{m}$, where only a couple of V-defects per device are expected. So far, there are no reports of $1 \mu\text{m}$ V-defect μ LEDs. Achieving a consistent performance across V-pit engineered $1 \mu\text{m}$ μ LEDs will likely require novel methods of V-pit formation, such that the μ LED mesas can be lithographically aligned to the V-pits.

A semi-relaxed InGaN pseudo-substrate (InGaNOs) was developed by Soitec based on its Smart CutTM technology.^{73,74} The lattice parameter of the InGaN layer can be increased to be 3.210 \AA , resulting in a reduction in compressive stress during the growth of InGaN quantum wells (QWs). The InGaN red QWs grown on such an InGaNOs template benefit from improved indium incorporation efficiency due to the compositional pulling effect, resulting in a much higher growth temperature of the InGaN red QWs (810°C) compared to that of InGaN red QWs (760°C) [Fig. 9(a)]. A significant redshift of $\sim 50 \text{ nm}$ in peak emission wavelength by photoluminescent was reported by Even *et al.* in 2017 from LETI and Soitec.⁷⁴ However, the native V-defect density is as high as

$5 \times 10^8 \text{ cm}^{-2}$ in the InGaNOs template, resulting in a low EQE of 0.14% for the red μ LEDs. Researchers from UCSB and Soitec have largely reduced the dislocation density using InGaN/GaN buffer/interlayer structure to achieve high crystal quality. Through these improvements and optimization of p-type InGaN epitaxy structure, the EQE of 609 nm InGaN red μ LEDs on InGaNOs has been enhanced to 0.83%.^{75,76}

Pasayat *et al.* from UCSB demonstrated compliant GaN on a patterned nano-porous GaN template, which facilitates strain relaxation in the upper overlaying InGaN layers.⁷⁷ The nano-porous GaN template is formed through electrochemical etching of the Si heavily doped n-GaN layer. Subsequent reactive ion etching (RIE) has a patterned nano-porous GaN template ($10 \times 10 \mu\text{m}^2$). A thick $\text{In}_{0.04}\text{Ga}_{0.96}\text{N}$ layer of $\sim 450 \text{ nm}$ was grown on top, achieving a strain relaxation of 56% [Fig. 9(b)]. This technique also induced a redshift in the emission wavelength of 56 nm. Ultra-small $6 \times 6 \mu\text{m}^2$ InGaN red μ LEDs (632 nm) were demonstrated with a peak on-wafer EQE of 0.2%. Issues such as thermal conductively and device's reliability become a concern for the InGaN red μ LEDs grown on the patterned nano-porous GaN template.

Chan *et al.* from UCSB reported a novel approach to achieve a highly strain-relaxed InGaN template. They utilized an *in situ* InGaN decomposition layer (DL) with a very high indium composition in the InGaN wells, which was subjected to rapid thermal annealing at 1000°C to induce void formation [Fig. 9(c)].⁷⁸ The

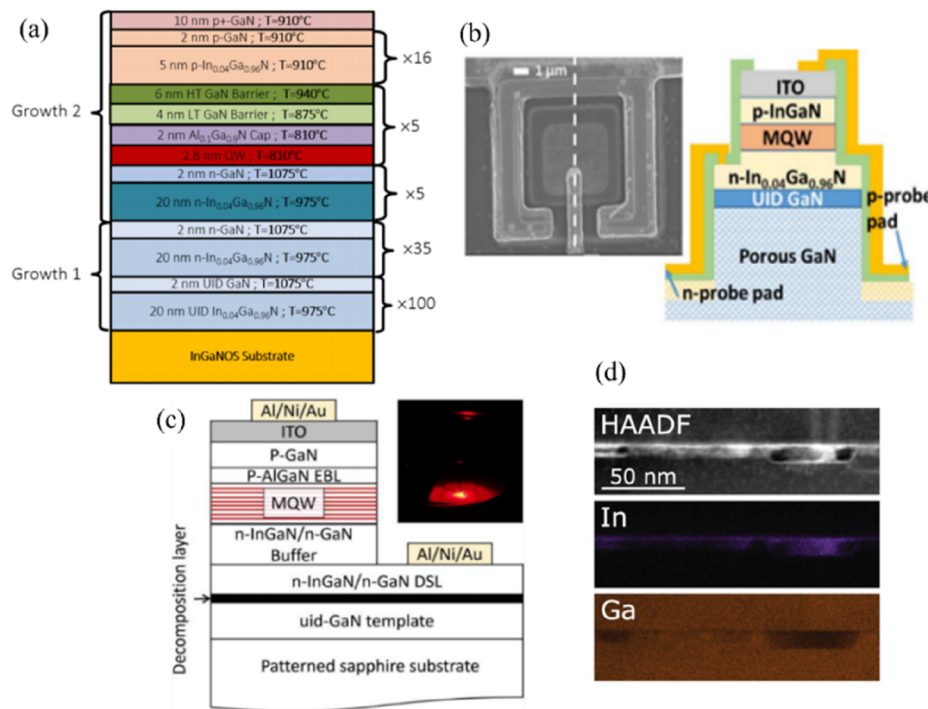


FIG. 9. (a) Cross section of red InGaN LED epilayer structure on the InGaNOs substrate.⁷⁶ (b) InGaN red μ LEDs on a nanoporous GaN template. Reproduced from Appl. Phys. Express **14**, 011004 (2021). Copyright IOP Publishing Ltd. All rights reserved. (c) InGaN red μ LEDs grown on an InGaN SRT template. Reproduced from Appl. Phys. Express **14**, 101002 (2021). Copyright IOP Publishing Ltd. All rights reserved. (d) TEM of the InGaN DL. Reproduced from White *et al.*, Appl. Phys. Lett. **119**, 131106 (2021) with the permission of AIP Publishing LLC.

embedded voids result in a very high biaxial relaxation of 85% in the 200 nm thick $\text{In}_{0.04}\text{Ga}_{0.96}\text{N}$ layer grown on top, leading to a large PL wavelength redshift of 75 nm (440 to 515 nm). The growth of the InGaN red QWs can be raised to a very high temperature of 850 °C and the red μLEDs exhibited on-wafer EQE of 0.05%.⁷⁹

InGaNOS, patterned nano-porous GaN template, and SRT with *in situ* DL are all developed with the goal of alleviating strain in the InGaN buffer layer and elevating the growth temperature for InGaN red QWs. However, InGaNOS and patterned nano-porous GaN template technology involve complicated procedures and materials overgrowth, resulting in a higher cost and a lower yield. SRT technology is a simple approach without taking the samples out of the reactor for extra overgrowth. However, the performance of the SRT InGaN red μLEDs remains poor. The dislocation density and the surface roughness of the $\text{In}_{0.04}\text{Ga}_{0.96}\text{N}$ SRT must be minimized to improve the efficiency of InGaN red μLEDs.

Other approaches such as ScAlMgO_4 and InGaN semi-bulk (SB) template were reported from red emission.^{97–99} ScAlMgO_4 , which has an in-plane lattice parameter of $a = 0.3249$ nm, is lattice matching with $\text{In}_{0.17}\text{Ga}_{0.83}\text{N}$ and a good candidate for long wavelength InGaN LEDs. Ozaki *et al.* from Kyoto University reported red emission from InGaN QWs with an indium composition higher than 20% grown on $\text{ScAlMgO}_4(0001)$ substrates with lattice-matched $\text{In}_{0.17}\text{Ga}_{0.83}\text{N}$ templates.⁹⁷ A high ratio of photoluminescence (PL) intensity of 0.14 at room temperature against that at 11 K was achieved, suggesting a promising IQE. However, the electrically injection red LEDs have not been demonstrated yet. Highly relaxed InGaN SB templates can reduce strain in the QWs grown on InGaN templates, resulting in an enhanced In-content due to the compositional pulling effect. Abdelhamid *et al.* shown a redshift at a peak emission wavelength of ~90 nm at low current injection for the InGaN LEDs grown on an $\text{In}_{0.12}\text{Ga}_{0.88}\text{N}$ SB template compared to the InGaN LEDs grown on a GaN template.⁹⁸ The same group also reported an improved LED output power and EQE using InGaN templates as compared to the LEDs grown on GaN substrates.⁹⁹ The SB template approach is a single step growth for the long wavelength LED structures. The main concern includes the material crystal quality of the $\text{In}_{0.12}\text{Ga}_{0.88}\text{N}$ SB template with a thickness of around 600 nm, which exceeds the critical thickness of $\text{In}_{0.12}\text{Ga}_{0.88}\text{N}$.¹⁰⁰

IV. GaN TJ-BASED CASCADED μLEDS FOR MONOLITHIC INTEGRATION

The development of III-nitride TJs for μLEDs is drawing significant interest due to several benefits, including an improved current spreading, reduced optical loss, and streamlined manufacturing.^{101–103} In addition, GaN TJ provides the feasibility of the cascaded μLED structure to integrate monolithic integration of multiple emission wavelengths.^{50,88} In this section, we will explore TJ μLEDs and the TJ enabled cascaded μLEDs configurations in greater detail.

A. TJ-based μLEDs

TJ are typically formed by growing a Si-heavily doped n^+ GaN on top of a heavily Mg doped p^+ GaN layer (Fig. 10). The operation of TJ μLEDs involves a distinct process: while the μLED operates

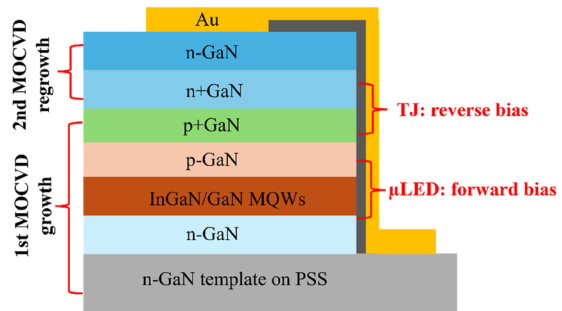


FIG. 10. Schematic structure of MOCVD-grown TJ μLEDs.

under a forward bias, electrons from the valence band of p-GaN tunnel into the conduction band of n-GaN, facilitating a hole injection into p-GaN.¹⁰¹ Metal–organic chemical vapor deposition (MOCVD) is commonly used as the industry standard for the mass production of III-nitride devices. However, MOCVD-grown TJ faces the challenge of thermal activation of Mg in the p-type layer: Mg was passivated by H during the overgrowth of n-GaN on top, which also prevents the out diffusion of H during the annealing process, making the full activation of p-type GaN very difficult.^{102,103} While sidewalls were commonly used as the pathways for H out diffusion, the lateral activation of Mg in the p-GaN is inefficient and the emission of μLEDs is nonuniform.^{102–109} In recent years, new innovations in the implementation of MOCVD-grown TJ μLEDs have been realized, such as selective area growth (SAG), the integration of $p^+\text{GaN}/\text{InGaN}/n^+\text{GaN}$ TJ, and sidewall chemical treatment. Researchers have successfully demonstrated full activation of Mg in the buried p-GaN, resulting in a notable reduction in voltage penalties, typically around 0.2 V.^{106,107}

In 2020, Li *et al.* from UCSB introduced size-independent voltage TJ μLEDs through SAG technology.¹⁰⁶ 210 nm thick SiO_2 pillars with a diameter of 1.5 μm and a space of 3.5 μm were used to form a hard mask on top of $p^+\text{GaN}$ in an LED wafer. In addition, $n^+\text{GaN}$ was selectively grown by MOCVD. The SiO_2 was removed by BHF, and very small holes were formed in $n^+\text{GaN}$ on top of the $p^+\text{GaN}$ surface, creating a natural out diffusion bypass for H. The voltage (V_f) of around 3.4 V is size-independent for the μLEDs size varied from 100×100 to $10 \times 10 \mu\text{m}^2$, suggesting that p-GaN was fully activated, since thermally activated H can diffuse a shorter distance to the exposed p-GaN vias.

The tunneling probability in a TJ according to the Wentzel–Kramers–Brillouin (WKB) approximation can be expressed by $T = \exp(-4\sqrt{2m_n E_g^{\frac{3}{2}}}/3q\hbar\varepsilon)$, where m_n is the electron effective mass, E_g is the bandgap energy, \hbar is the Planck constant, and ε is the electric field. Due to GaN's large bandgap energy of 3.4 eV, the tunneling probability is much lower compared to other materials, such as Si and Ge. In 2020, Li *et al.* from UCSB demonstrated high performance TJ μLEDs using a $n^+\text{GaN}/\text{InGaN}/p^+\text{GaN}$ TJ structure.¹¹⁰ By incorporating a thin (3 nm) $\text{In}_{0.15}\text{Ga}_{0.85}\text{N}$ layer, tunneling probability is significantly increased, resulting in a reduction of V_f by 0.6 V in TJ μLEDs. The excess voltage of TJ μLEDs was only ~0.2 V higher than that of the common μLEDs with ITO contact. Despite potential absorption of emission light by a very thin 3 nm InGaN insertion

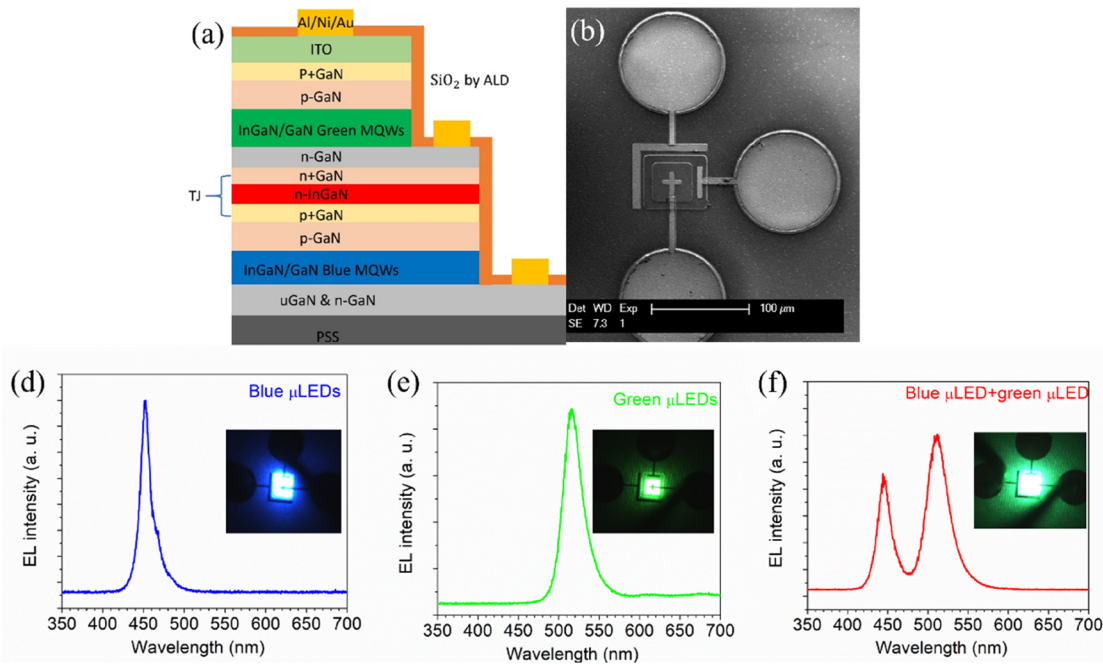


FIG. 11. Panels (a) and (b): TJ-based vertically cascaded μLEDs stack. Panels (c)–(e) are the emission spectra from the vertically cascaded μLEDs stack. Reproduced from Li *et al.*, Appl. Phys. Lett. **118**, 261104 (2021) with the permission of AIP Publishing LLC.

layer, the InGaN TJ μLEDs show an enhanced output power due to a reduced light loss.

Wong *et al.* from UCSB show that chemical treatment prior to sidewall activation enables homogeneous electroluminescence (EL) emission from the MOCVD-grown TJ μLEDs.¹¹ The chemical treatment involved three cycles of 5 min of phosphoric acid at 60 °C, 5 min of ultraviolet-ozone treatment, and 5 min of hydrofluoric acid, followed by thermal annealing for 30 min. The applied chemical treatments removed the damaged sidewall material that inhibited efficient activation of p-GaN. This method is effective for TJ μLEDs smaller than 40 × 40 μm² as it still relies on lateral sidewall activation.

B. III-nitride TJ-based cascaded μLEDs for monolithic integration

The low-voltage penalty of TJ μLEDs utilizes an advanced μLEDs cascaded μLEDs structure. In this configuration, a series of LED can be connected via TJ within a single epitaxial structure. Essentially, TJ offers the design of the cascade μLEDs design to achieve monolithic integration of multiple emission wavelengths μLEDs.

In 2021, Li *et al.* from UCSB demonstrated highly efficient cascaded InGaN-based blue and green μLEDs stacks. This structure comprised blue μLEDs, TJ, and green μLEDs [Figs. 11(a) and 11(b)].^{50,107} The epitaxial stacks, including a 450 nm blue LED, InGaN TJ, and 518 nm InGaN were fully grown by MOCVD. Innovation in the implementation of independent μLEDs junction

control was realized using three electrodes. By aligning the valence and conduction bands of neighboring layers, two-way tunneling of electrons through a very thin depletion region is allowed. Current can flow through a reverse *pn* junction through the TJ. The blue μLEDs and green μLEDs were controlled independently [Figs. 11(c)–11(e)], showing a high peak EQE of 42% and 14%, respectively. More recently, Saito *et al.* from Meijo University reported a monolithic III-nitride RGB μLEDs array composed of InGaN blue, green, and red μLEDs horizontally stacked on the same wafer.¹¹² The TJ-based cascaded μLEDs technology shows significant advancements in native InGaN-based RGB directionality and pixel size reduction, presenting an innovative solution to overcome the mass transfer of ultra-small RGB μLEDs for AR display.

V. CONCLUSION AND OUTLOOK

In summary, we discussed the critical challenges of ultra-small μLEDs for AR displays and explored the possible solutions. Novel self-alignment process technology has been developed to realize efficient InGaN blue and green μLEDs scaled to 1 μm. The efficiency of InGaN-based red μLEDs has recently been improved significantly. The efficiency of ultra-small InGaN red μLEDs would outperform the conventional AlInGaP red μLEDs due to a reduced surface recombination velocity. Other challenges of InGaN red μLEDs, such as broad spectra and blueshift in peak wavelength, need to be addressed for the AR display. III-nitride TJ enables the realization of cascaded InGaN μLEDs and provides a new opportunity of monolithic integration full-color RGB InGaN μLEDs, making it feasible

to save the huge efforts to mass transfer RGB μLEDs from three different epitaxy wafers.

ACKNOWLEDGMENTS

The authors acknowledge the Solid-State Lighting and Energy Electronics Center (SSLEEC) at UCSB for partially funding this work. A portion of this work was done at the UCSB nanofabrication facility and the Materials Research Laboratories.

AUTHOR DECLARATIONS

Conflict of Interest

The authors have no conflicts to disclose.

Author Contributions

Panpan Li: Conceptualization (equal); Data curation (equal); Formal analysis (equal); Investigation (equal); Methodology (equal); Project administration (equal); Resources (equal); Software (equal); Writing – original draft (equal); Writing – review & editing (equal).

Jacob Ewing: Conceptualization (equal); Formal analysis (equal); Investigation (equal); Resources (equal); Writing – original draft (equal); Writing – review & editing (equal). **Matthew S. Wong:** Conceptualization (equal); Formal analysis (equal); Resources (equal); Writing – original draft (equal); Writing – review & editing (equal).

Yifan Yao: Formal analysis (equal); Investigation (equal); Methodology (equal); Resources (equal); Writing – original draft (equal); Writing – review & editing (equal). **Hongjian Li:** Conceptualization (equal); Data curation (equal); Formal analysis (equal); Investigation (equal); Writing – original draft (equal); Writing – review & editing (equal).

Srinivas Gandrothula: Formal analysis (equal); Investigation (equal); Writing – original draft (equal); Writing – review & editing (equal). **Jordan M. Smith:** Data curation (equal); Resources (equal). **Mike Iza:** Investigation (equal); Resources (equal). **Shuji Nakamura:** Conceptualization (equal); Funding acquisition (equal); Investigation (equal); Project administration (equal); Supervision (equal); Writing – review & editing (equal). **Steven P. DenBaars:** Conceptualization (lead); Formal analysis (lead); Funding acquisition (lead); Investigation (lead); Methodology (equal); Project administration (lead); Supervision (equal); Writing – original draft (equal); Writing – review & editing (equal).

DATA AVAILABILITY

The data that support the findings of this study are available from the corresponding author upon reasonable request.

REFERENCES

- ¹J. Day, J. Li, D. Y. C. Lie, C. Bradford, J. Y. Lin, and H. X. Jiang, *Appl. Phys. Lett.* **99**, 031116 (2011).
- ²Y. Huang, E.-L. Hsiang, M.-Y. Deng, and S.-T. Wu, *Light Sci. Appl.* **9**, 105 (2020).
- ³E.-L. Hsiang, Z. Yang, Q. Yang, Y.-F. Lan, and S.-T. Wu, *J. Soc. Inf. Disp.* **29**, 446 (2021).
- ⁴G. Tan, Y.-H. Lee, T. Zhan, J. Yang, S. Liu, D. Zhao, and S.-T. Wu, *Opt. Express* **26**, 025076 (2018).
- ⁵J. J. Wierer, Jr. and N. Tansu, *Laser Photonics Rev.* **13**, 1900141 (2019).
- ⁶X. Zhang, Z. Li, Y. Zhang, X. Wang, X. Yi, G. Wang, and J. Li, *Opt. Express* **30**, 26676 (2022).
- ⁷K. Fan, K. Zheng, J. Lv, B. Zhao, Y. Zhao, Y. Chen, Y. Qin, Q. Wang, W. Wang, and J. Liang, *Opt. Express* **31**, 36293 (2023).
- ⁸Y. Yao, H. Li, P. Li, C. J. Zollner, M. Wang, M. Iza, J. S. Speck, S. P. DenBaars, and S. Nakamura, *Appl. Phys. Express* **15**, 064003 (2022).
- ⁹S. Gandrothula, T. Kamikawa, P. Shapurekha, R. Anderson, M. Wong, H. Zhang, J. S. Speck, S. Nakamura, and S. P. Denbaars, *Appl. Phys. Lett.* **119**, 142103 (2021).
- ¹⁰F. Olivier, S. Tirano, L. Dupré, B. Aventurier, C. Largeron, and F. Templier, *J. Lumin.* **191**, 112 (2017).
- ¹¹D. Hwang, A. Mughal, C. D. Pynn, S. Nakamura, and S. P. DenBaars, *Appl. Phys. Express* **10**, 032101 (2017).
- ¹²P. Tian, J. J. D. McKendry, J. Herrnsdorf, S. Watson, R. Ferreira, I. M. Watson, E. Gu, A. E. Kelly, and M. D. Dawson, *Appl. Phys. Lett.* **105**, 4 (2014).
- ¹³M. S. Wong, C. Lee, D. J. Myers, D. Hwang, J. A. Kearns, T. Li, J. S. Speck, S. Nakamura, and S. P. Denbaars, *Appl. Phys. Express* **12**, 097004 (2019).
- ¹⁴T.-Y. Lee, L.-Y. Chen, Y.-Y. Lo, S. S. Swayamprabha, A. Kumar, Y.-M. Huang, S.-C. Chen, H.-W. Zan, F.-C. Chen, R.-H. Horng, and H.-C. Kuo, *ACS Photonics* **9**(9), 2905 (2022).
- ¹⁵F. Olivier, A. Daami, C. Licita, and F. Templier, *Appl. Phys. Lett.* **111**, 022104 (2017).
- ¹⁶M. S. Wong, S. Nakamura, and S. P. DenBaars, *ECS J. Solid State Sci. Technol.* **9**, 015012 (2020).
- ¹⁷J. Y. Lin and H. X. Jiang, *Appl. Phys. Lett.* **116**, 100502 (2020).
- ¹⁸J. M. Smith, R. Ley, M. S. Wong, Y. H. Baek, J. H. Kang, C. H. Kim, M. J. Gordon, S. Nakamura, J. S. Speck, and S. P. Denbaars, *Appl. Phys. Lett.* **116**, 071102 (2020).
- ¹⁹K. Bulashevich, S. Konoplev, and S. Karpov, *Photonics* **5**, 41 (2018).
- ²⁰J.-T. Oh, S.-Y. Lee, Y.-T. Moon, J. H. Moon, S. Park, K. Y. Hong, K. Y. Song, C. Oh, J.-I. Shim, H.-H. Jeong, J.-O. Song, H. Amano, and T.-Y. Seong, *Opt. Express* **26**, 11194 (2018).
- ²¹K. A. Bulashevich and S. Y. Karpov, *Phys. Status Solidi RRL* **10**, 480 (2016).
- ²²J. Kou, C.-C. Shen, H. Shao, J. Che, X. Hou, C. Chu, K. Tian, Y. Zhang, Z.-H. Zhang, and H.-C. Kuo, *Opt. Express* **27**, 643 (2019).
- ²³J. Back, M. S. Wong, J. Kearns, S. P. DenBaars, C. Weisbuch, and S. Nakamura, *Opt. Express* **28**, 29991 (2020).
- ²⁴K. Zhang, T. Takahashi, D. Ohori, G. Cong, K. Endo, N. Kumagai, S. Samukawa, M. Shimizu, and X. Wang, *Semicond. Sci. Technol.* **35**, 075001 (2020).
- ²⁵Z. Chen, S. Yan, and C. Danesh, *J. Phys. D Appl. Phys.* **54**, 123001 (2021).
- ²⁶J. Slawinska, G. Muziol, M. Siekacz, H. Turski, M. Hajdel, M. Zak, A. Feduniewicz-Zmuda, G. Staszczak, and C. Skierbiszewski, *Opt. Express* **30**, 27004 (2022).
- ²⁷M. S. Wong, D. Hwang, A. I. Alhassan, C. Lee, R. Ley, S. Nakamura, and S. P. DenBaars, *Opt. Express* **26**, 21324 (2018).
- ²⁸J.-H. Park, M. Pristovsek, H. Amano, and T.-Y. Seong, *Appl. Phys. Rev.* **11**, 021319 (2024).
- ²⁹M.-C. Wu, Z.-L. Hsu, and C.-Y. Wu, *IEEE Trans. Electron Devices* **69**, 6206 (2022).
- ³⁰S. Lan, H. Wan, J. Zhao, and S. Zhou, *Micromachines* **10**, 860 (2019).
- ³¹T. Ma, J. Chen, Z. Chen, L. Liang, J. Hu, W. Shen, Z. Li, and H. Zeng, *Adv. Mater. Technol.* **8**, 2200632 (2023).
- ³²L. Qi, P. Li, X. Zhang, K. M. Wong, and K. M. Lau, *Light Sci. Appl.* **12**, 258 (2023).
- ³³K.-L. Liang, W.-H. Kuo, H.-T. Shen, P.-W. Yu, Y.-H. Fang, and C.-C. Lin, *Jpn. J. Appl. Phys.* **60**, SA0802 (2021).
- ³⁴M. Boroditsky, I. Gontijo, M. Jackson, R. Vrijen, E. Yablonovitch, T. Krauss, C.-C. Cheng, A. Scherer, R. Bhat, and M. Krames, *J. Appl. Phys.* **87**, 3497 (2000).
- ³⁵Z. Lu, K. Zhang, J. Zhuang, J. Lin, Z. Lu, Z. Jiang, Y. Lu, Z. Chen, and W. Guo, *Micro Nanostruct.* **183**, 207669 (2023).
- ³⁶J. Ryu, S. Park, Y. Park, S. Ryu, K. Hwang, and H. W. Jang, *Adv. Mater.* **35**, 2204947 (2023).
- ³⁷J. Bae, Y. Shin, H. Yoo, Y. Choi, J. Lim, D. Jeon, I. Kim, M. Han, and S. Lee, *Nat. Commun.* **13**, 1862 (2022).

- ³⁸Y. Narukawa, M. Ichikawa, D. Sanga, M. Sano, and T. Mukai, *J. Phys. D: Appl. Phys.* **43**, 354002 (2010).
- ³⁹P. Li, Y. Zhao, H. Li, J. Che, Z. Zhang, Z. Li, Y. Zhang, L. Wang, M. Liang, X. Yi, and G. Wang, *Opt. Express* **26**, 33108 (2018).
- ⁴⁰Z. Chen, B. Sheng, F. Liu, S. Liu, D. Li, Z. Yuan, T. Wang, X. Rong, J. Huang, J. Qiu, W. Liang, C. Zhao, L. Yan, J. Hu, S. Guo, W. Ge, B. Shen, and X. Wang, *Adv. Funct. Mater.* **33**, 2300042 (2023).
- ⁴¹F. Liu, Y. Yu, Y. T. Zhang, X. Rong, T. Wang, X. T. Zheng, B. W. Sheng, L. Y. Yang, J. Q. Wei, X. P. Wang, X. B. Li, X. L. Yang, F. J. Xu, Z. X. Qin, Z. H. Zhang, B. Shen, and X. Q. Wang, *Adv. Sci.* **7**, 2000917 (2020).
- ⁴²H. Li, M. S. Wong, M. Khoury, B. Bonef, H. Zhang, Y. Chow, P. Li, J. Kearns, A. A. Taylor, P. De Mierry, Z. Hassan, S. Nakamura, and S. P. DenBaars, *Opt. Express* **27**, 24154 (2019).
- ⁴³Y. Zhao, S. Tanaka, Q. Yan, C. Y. Huang, R. B. Chung, C. C. Pan, K. Fujito, D. Feezell, C. G. Van de Walle, J. S. Speck, S. P. DenBaars, and S. Nakamura, *Appl. Phys. Lett.* **99**, 051109 (2011).
- ⁴⁴Y. Wu, J. Ma, P. Su, L. Zhang, and B. Xia, *Nanomaterials* **10**, 2482 (2020).
- ⁴⁵D. Lee, S. Cho, C. Park, K. R. Park, J. Lee, J. Nam, K. Ahn, C. Park, K. Jeon, H. Yuh, W. Choi, C. H. Lim, T. Kwon, Y. H. Min, M. Joo, Y.-H. Choi, J. S. Lee, C. Kim, and S. Kwon, *Nature* **619**, 755 (2023).
- ⁴⁶F. Chen, J. Bian, J. Hu, N. Sun, B. Yang, H. Ling, H. Yu, K. Wang, M. Gai, Y. Ma, and Y. Huang, *Int. J. Extreme Manuf.* **4**, 042005 (2022).
- ⁴⁷H. Lu, W. Guo, C. Su, X. Li, Y. Lu, L. Zhu, and Z. Chen, *IEEE J. Electron Devices Soc.* **8**, 554 (2020).
- ⁴⁸N. Yulianto, A. D. Refino, A. Syring, N. Majid, S. Mariana, P. Schnell, R. A. Wahyuno, K. Triyana, F. Meierhofer, W. Daum, F. F. Abdi, T. Voss, H. S. Wasisto, and A. Waag, *Microsyst. Nanoeng.* **7**, 1 (2021).
- ⁴⁹N. Yulianto, G. T. M. Kadja, S. Bornemann, S. Gahlawat, N. Majid, K. Triyana, F. F. Abdi, H. S. Wasisto, and A. Waag, *ACS Appl. Electron. Mater.* **3**, 778 (2021).
- ⁵⁰P. Li, H. Li, Y. Yao, H. Zhang, C. Lynsky, K. S. Qwah, J. S. Speck, S. Nakamura, and S. P. DenBaars, *Appl. Phys. Lett.* **118**, 261104 (2021).
- ⁵¹M. S. Wong, S. Gee, T. Tak, S. Gandrothula, S. Rebollo, N. Cha, J. S. Speck, and S. P. DenBaars, *Jpn. J. Appl. Phys.* **63**, 040903 (2024).
- ⁵²S.-W. Huang Chen, C.-C. Shen, T. Wu, Z.-Y. Liao, L.-F. Chen, J.-R. Zhou, C.-F. Lee, C.-H. Lin, C.-C. Lin, C.-W. Sher, P.-T. Lee, A.-J. Tzou, Z. Chen, and H.-C. Kuo, *Photonics Res.* **7**, 416 (2019).
- ⁵³M. Sheen, Y. Ko, D. Kim, J. Kim, J. H. Byun, Y. S. Choi, J. Ha, K. Y. Yeon, D. Kim, J. Jung, J. Choi, R. Kim, J. Yoo, I. Kim, C. Joo, N. Hong, J. Lee, S. H. Jeon, S. H. Oh, J. Lee, N. Ahn, and C. Lee, *Nature* **608**, 56 (2022).
- ⁵⁴J. Yu, T. Tao, B. Liu, F. Xu, Y. Zheng, X. Wang, Y. Sang, Y. Yan, Z. Xie, S. Liang, D. Chen, P. Chen, X. Xiu, Y. Zheng, and R. Zhang, *Crystals* **11**, 1 (2021).
- ⁵⁵Y. Yue, X. Yan, W. Li, H. G. Xing, D. Jena, and P. Fay, *J. Vac. Sci. Technol., B* **32**, 061201 (2014).
- ⁵⁶Y. Yang and X. A. Cao, *J. Vac. Sci. Technol. B* **27**, 2337 (2009).
- ⁵⁷C. L. Maoulit, D. Vaufrey, F. F. Martin, E. E. Martinez, E. Nolot, S. S. Cadot, and E. Gheeraert, *Proc. SPIE* **11280**, 46 (2020).
- ⁵⁸S. Finot, C. Le Maoulit, E. Gheeraert, D. Vaufrey, and G. Jacopin, *ACS Photonics* **9**, 173 (2022).
- ⁵⁹H. M. Kim, C. Huh, S. W. Kim, N. M. Park, and S. J. Park, *Electrochem. Solid-State Lett.* **7**, 241 (2004).
- ⁶⁰B. Tang, J. Miao, Y. Liu, H. Wan, N. Li, S. Zhou, and C. Gui, *Nanomaterials* **9**, 319 (2019).
- ⁶¹A. Pandey, J. Min, M. Reddeppa, Y. Malhotra, Y. Xiao, Y. Wu, K. Sun, and Z. Mi, *Nano Lett.* **23**, 1680 (2023).
- ⁶²R. T. Ley, J. M. Smith, M. S. Wong, T. Margalith, S. Nakamura, S. P. DenBaars, and M. J. Gordon, *Appl. Phys. Lett.* **116**, 251104 (2020).
- ⁶³P. Li, H. Li, H. Zhang, C. Lynsky, M. Iza, J. S. Speck, S. Nakamura, and S. P. DenBaars, *Appl. Phys. Lett.* **119**, 081102 (2021).
- ⁶⁴D.-H. Lee, S.-Y. Lee, J.-I. Shim, T.-Y. Seong, and H. Amano, *ECS J. Solid State Sci. Technol.* **10**, 095001 (2021).
- ⁶⁵P. Li, A. David, H. Li, H. Zhang, C. Lynsky, Y. Yang, M. Iza, J. S. Speck, S. Nakamura, and S. P. DenBaars, *Appl. Phys. Lett.* **119**, 231101 (2021).
- ⁶⁶A. David, C. A. Hurni, N. G. Young, and M. D. Craven, *Appl. Phys. Lett.* **109**, 083501 (2016).
- ⁶⁷P. Li, H. Li, Y. Yao, N. Lim, M. Wong, M. Iza, M. Gordon, J. S. Speck, S. Nakamura, and S. P. DenBaars, *ACS Photonics* **10**, 1899 (2023).
- ⁶⁸D. Lee, Y. Choi, S. Jung, Y. Kim, S. Park, P. Choi, and S. Yoon, *Appl. Phys. Lett.* **124**, 121109 (2024).
- ⁶⁹F. Jiang, J. Zhang, L. Xu, J. Ding, G. Wang, X. Wu, X. Wang, C. Mo, Z. Quan, X. Guo, C. Zheng, S. Pan, and J. Liu, *Photonics Res.* **7**, 144 (2019).
- ⁷⁰D. Iida, Z. Zhuang, P. Kirilenko, M. Velazquez-Rizo, M. A. Najmi, and K. Ohkawa, *Appl. Phys. Lett.* **116**, 162101 (2020).
- ⁷¹Z. Zhuang, D. Iida, M. Velazquez-Rizo, and K. Ohkawa, *Photonics Res.* **9**, 1796 (2021).
- ⁷²D. Iida, P. Kirilenko, M. Velazquez-Rizo, Z. Zhuang, M. A. Najmi, and K. Ohkawa, *AIP Adv.* **12**, 065125 (2022).
- ⁷³A. Even, G. Laval, O. Ledoux, P. Ferret, D. Sotta, E. Guiot, F. Levy, I. C. Robin, and A. Dussaigne, *Appl. Phys. Lett.* **110**, 262103 (2017).
- ⁷⁴A. Dussaigne, P. Le Maitre, H. Haas, J.-C. Pillet, F. Barbier, A. Grenier, N. Michit, A. Jannaud, R. Templier, D. Vaufrey, F. Rol, O. Ledoux, and D. Sotta, *Appl. Phys. Express* **14**, 092011 (2021).
- ⁷⁵R. C. White, M. Khoury, M. S. Wong, H. Li, C. Lynsky, M. Iza, S. Keller, D. Sotta, S. Nakamura, and S. P. DenBaars, *Crystals* **11**, 1168 (2021).
- ⁷⁶R. C. White, H. Li, M. Khoury, C. Lynsky, M. Iza, S. Keller, D. Sotta, S. Nakamura, and S. P. DenBaars, *Crystals* **11**, 1364 (2021).
- ⁷⁷S. S. Pasayat, C. Gupta, M. S. Wong, R. Ley, M. J. Gordon, S. P. DenBaars, S. Nakamura, S. Keller, and U. K. Mishra, *Appl. Phys. Express* **14**, 011004 (2021).
- ⁷⁸P. Chan, V. Rienzi, N. Lim, H. M. Chang, M. Gordon, S. P. DenBaars, and S. Nakamura, *Appl. Phys. Express* **14**, 101002 (2021).
- ⁷⁹P. Chan, S. P. DenBaars, and S. Nakamura, *Appl. Phys. Lett.* **119**, 131106 (2021).
- ⁸⁰J.-I. Hwang, R. Hashimoto, S. Saito, and S. Nunoue, *Appl. Phys. Express* **7**, 071003 (2014).
- ⁸¹P. Li, H. Li, Y. Yang, H. Zhang, P. Shapurenska, M. Wong, C. Lynsky, M. Iza, M. J. Gordon, J. S. Speck, S. Nakamura, and S. P. DenBaars, *Appl. Phys. Lett.* **120**, 041102 (2022).
- ⁸²N. Horiuchi, *Nat. Photonics* **16**, 264 (2022).
- ⁸³P. Li, H. Li, Y. Yang, M. Wong, M. Iza, M. J. Gordon, J. S. Speck, S. Nakamura, and S. P. DenBaars, *Appl. Phys. Express* **16**, 064002 (2023).
- ⁸⁴Z. Jiang, Y. Jiang, M. Chen, J. Li, P. Li, B. Chen, S. Zhao, J. Wang, S. Jiang, M. Cai, L. Li, C. Li, K. Huang, W. Lu, J. Kang, and R. Zhang, *Laser Photonics Rev.* **17**, 2300113 (2023).
- ⁸⁵C. Lynsky, A. I. Alhassan, G. Lheureux, B. Bonef, S. P. DenBaars, S. Nakamura, Y.-R. Wu, C. Weisbuch, and J. S. Speck, *Phys. Rev. Mater.* **4**, 054604 (2020).
- ⁸⁶X. H. Wu, C. R. Elsass, A. Abare, M. Mack, S. Keller, P. M. Petroff, S. P. DenBaars, J. S. Speck, and S. J. Rosner, *Appl. Phys. Lett.* **72**, 692 (1998).
- ⁸⁷S. Zhang, J. Zhang, J. Gao, X. Wang, C. Zheng, M. Zhang, X. Wu, L. Xu, J. Ding, Z. Quan, and F. Jiang, *Photonics Res.* **8**, 1671 (2020).
- ⁸⁸R. Armitage, Z. Ren, M. Holmes, and J. Flemish, *Phys. Status Solidi RRL* **2024**, 2400012 (2024).
- ⁸⁹C.-K. Li, C.-K. Wu, C.-C. Hsu, L.-S. Lu, H. Li, T.-C. Lu, and Y.-R. Wu, *AIP Adv.* **6**, 055208 (2016).
- ⁹⁰F. Wu, J. Ewing, C. Lynsky, M. Iza, S. Nakamura, S. P. DenBaars, and J. S. Speck, *J. Appl. Phys.* **133**, 035703 (2023).
- ⁹¹S. Marcinkevičius, J. Ewing, R. Yapparov, F. Wu, S. Nakamura, and J. S. Speck, *Appl. Phys. Lett.* **123**, 201102 (2023).
- ⁹²J. Ewing, C. Lynsky, J. Zhang, P. Shapurenska, M. Wong, J. Smith, M. Iza, J. S. Speck, and S. P. DenBaars, *Crystals* **12**, 1216 (2022).
- ⁹³J. J. Ewing, C. Lynsky, M. S. Wong, F. Wu, Y. C. Chow, P. Shapurenska, M. Iza, S. Nakamura, S. P. DenBaars, and J. S. Speck, *Opt. Express* **31**, 41351 (2023).
- ⁹⁴C. H. Ho, J. S. Speck, C. Weisbuch, and Y.-R. Wu, *Phys. Rev. Appl.* **17**, 014033 (2022).
- ⁹⁵T. Tak, C. W. Johnson, W. Y. Ho, F. Wu, M. Sauty, S. Rebollo, A. K. Schmid, J. Peretti, Y.-R. Wu, C. Weisbuch, and J. S. Speck, *Phys. Rev. Appl.* **20**, 064045 (2023).
- ⁹⁶J. Ewing *et al.*, *Phys. Rev. Appl.* **21**, 064042 (2024).
- ⁹⁷T. Ozaki, M. Funato, and Y. Kawakami, *Appl. Phys. Express* **12**, 011007 (2019).
- ⁹⁸M. Abdelhamid, E. L. Routh, A. Shaker, and S. M. Bedair, *Superlattices Microstruct.* **160**, 107065 (2021).

- ⁹⁹M. Abdelhamid, E. L. Routh, B. Hagar, and S. M. Bedair, *Appl. Phys. Lett.* **120**, 081104 (2022).
- ¹⁰⁰M. Leyer, J. Stellmach, Ch. Meissner, M. Pristovsek, and M. Kneissl, *J. Cryst. Growth* **310**, 4913 (2008).
- ¹⁰¹B. P. Yonkee, E. C. Young, S. P. DenBaars, S. Nakamura, and J. S. Speck, *Appl. Phys. Lett.* **109**, 191104 (2016).
- ¹⁰²Y. Kuwano, M. Kaga, T. Morita, K. Yamashita, K. Yagi, M. Iwaya, T. Takeuchi, S. Kamiyama, and I. Akasaki, *Jpn. J. Appl. Phys.* **52**, 08JK12 (2013).
- ¹⁰³Z. Jamal-Eddine, S. M. N. Hasan, B. Gunning, H. Chandrasekar, M. Crawford, A. Armstrong, S. Arafin, and S. Rajan, *Appl. Phys. Lett.* **117**, 051103 (2020).
- ¹⁰⁴Y. Zhang, Z. J. Eddine, and S. Rajan, *Jpn. J. Appl. Phys.* **58**, SC0805 (2019).
- ¹⁰⁵T. Takeuchi, S. Kamiyama, M. Iwaya, and I. Akasaki, *Semicond. Sci. Technol.* **36**, 063001 (2021).
- ¹⁰⁶P. Li, H. Zhang, H. Li, M. Iza, Y. Yao, M. S. Wong, N. Palmquist, J. S. Speck, S. Nakamura, and S. P. DenBaars, *Opt. Express* **28**, 18707 (2020).
- ¹⁰⁷P. Li, H. Li, Y. Yao, H. Zhang, C. Lynsky, K. S. Qwah, M. Iza, J. S. Speck, S. Nakamura, and S. P. DenBaars, *Opt. Express* **29**, 22001 (2021).
- ¹⁰⁸S. M. N. Hasan, B. P. Gunning, Z. J-Eddine, H. Chandrasekar, M. H. Crawford, A. Armstrong, S. Rajan, and S. Arafin, *J. Phys. D: Appl. Phys.* **54**, 155103 (2021).
- ¹⁰⁹Y. Akatsuka, S. Iwayama, T. Takeuchi, S. Kamiyama, M. Iwaya, and I. Akasaki, *Appl. Phys. Express* **12**, 025502 (2019).
- ¹¹⁰P. Li, H. Zhang, H. Li, Y. Zhang, Y. Yao, N. Palmquist, M. Iza, J. Speck, S. Nakamura, and S. P. DenBaars, *Semicond. Sci. Technol.* **35**, 125023 (2020).
- ¹¹¹M. S. Wong, N. C. Palmquist, J. Jiang, P. Chan, C. Lee, P. Li, J. H. Kang, Y. H. Baek, C. H. Kim, D. A. Cohen, T. Margalith, J. S. Speck, S. Nakamura, and S. P. DenBaars, *Appl. Phys. Lett.* **119**, 202102 (2021).
- ¹¹²T. Saito, N. Hasegawa, K. Imura, Y. Suehiro, T. Takeuchi, S. Kamiyama, D. Iida, K. Ohkawa, and M. Iwaya, *Appl. Phys. Express* **16**, 084001 (2023).